JACS
JOURNAL OF THE AMERICAN CHEMICAL SOCIETY

Article

pubs.acs.org/JACS

Anomalous Self-Diffusion and Sticky Rouse Dynamics in Associative Protein Hydrogels

Shengchang Tang, Muzhou Wang, and Bradley D. Olsen*

Department of Chemical Engineering, Massachusetts Institute of Technology, 77 Massachusetts Avenue, Cambridge, Massachusetts 02139, United States

Supporting Information

ABSTRACT: Natural and synthetic materials based on associating polymers possess diverse mechanical behavior, transport properties and responsiveness to external stimuli. Although much is known about their dynamics on the molecular and macroscopic level, knowledge of self-diffusive dynamics of the network-forming constituents remains limited. Using forced Rayleigh scattering, anomalous self-diffusion is observed in model associating protein hydrogels originating from the interconversion between species that diffuse in both the molecular and associated state. The diffusion can be quantitatively modeled using a two-state model for polymers in the gel, where diffusivity in the associated state is critical to the super diffusive behavior. The dissociation time from bulk rheology measurements was 2−3 orders of magnitude smaller than the one measured by diffusion, because the former characterizes submolecular dissociation dynamics, whereas the latter depicts single protein molecules completely disengaging from the network. Rheological data also show a sticky Rouse-like relaxation at long times due to collective relaxation of large groups of proteins, suggesting mobility of associated molecules. This study experimentally demonstrates a hierarchy of relaxation processes in associating polymer networks, and it is anticipated that the results can be generalized to other associative systems to better understand the relationship of dynamics among sticky bonds, single molecules, and the entire network.

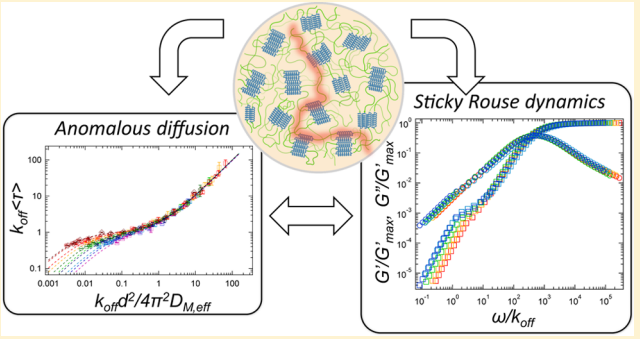

INTRODUCTION

Natural and synthetic materials based upon associating networks are of longstanding interest across a wide variety of different communities.[1,2] These materials share a common feature that the network junctions are formed by various physical or supramolecular interactions, including hydrogen bonding,[3−5] metal−ligand coordination,[6−8] ionic interactions (coacervation),[9,10] hydrophobic interactions,[11,12] host−guest complexation,[13,14] and combinations thereof in intricate self-assembled systems.[15−18] Since the association energies of the physical bonds are typically on the order of a few to tens of k_BT (the thermal energy),[19] these bonds can dissociate and recombine due to thermal fluctuation or when triggered by mild environmental stimuli. This feature distinguishes associating networks from their chemically cross-linked counterparts and gives rise to many interesting transport and mechanical properties. For example, the nuclear pore complex uses weak associations between proteins to regulate the transport of molecules into the nucleus.[20] Many researchers have incorporated associating bonds into materials to prepare batteries,[21] conductive artificial skin,[22] elastomers,[5,23,24] and soft hydrogels[6] with self-healing properties. The associative junctions can also serve as sacrificial bonds for effective energy dissipation in order to prevent concentrated stress at the early stage of the stretch, enabling soft materials to achieve dramatic enhancements in toughness.[25,26] Moreover, biocompatible associating gels have shown significant promise as injectable cell-encapsulating materials for medical applications.[27,28]

Network dynamics are important to control the materials' properties, such as the time scale of self-healing,[5] the susceptibility to creep at long time,[29,30] and the influence of relaxation time of synthetic microenvironments on cell response.[31] From a fundamental perspective, the dynamics of an entire network are largely controlled by the dynamics of associating bonds or stickers. This has provided the basis for many theoretical models developed throughout the past seven decades.[32−39] In particular, the sticky Rouse/reptation theories are suitable to describe the dynamics of polymers with associating side groups along the backbone.[35] These theories reason that the presence of the stickers introduces additional friction between polymers, and such effect is enhanced drastically with increasing sticker density. As a result, the dynamics (e.g., relaxation time, self-diffusivity, and zero-shear-rate viscosity) of associating polymers strongly depends on the number of stickers per chain, the polymer concentration, and the polymer architecture. This complexity makes it difficult to

Received: January 21, 2015
Published: March 12, 2015

DOI: 10.1021/jacs.5b00722
J. Am. Chem. Soc. 2015, 137, 3946−3957

Scheme 1[a]

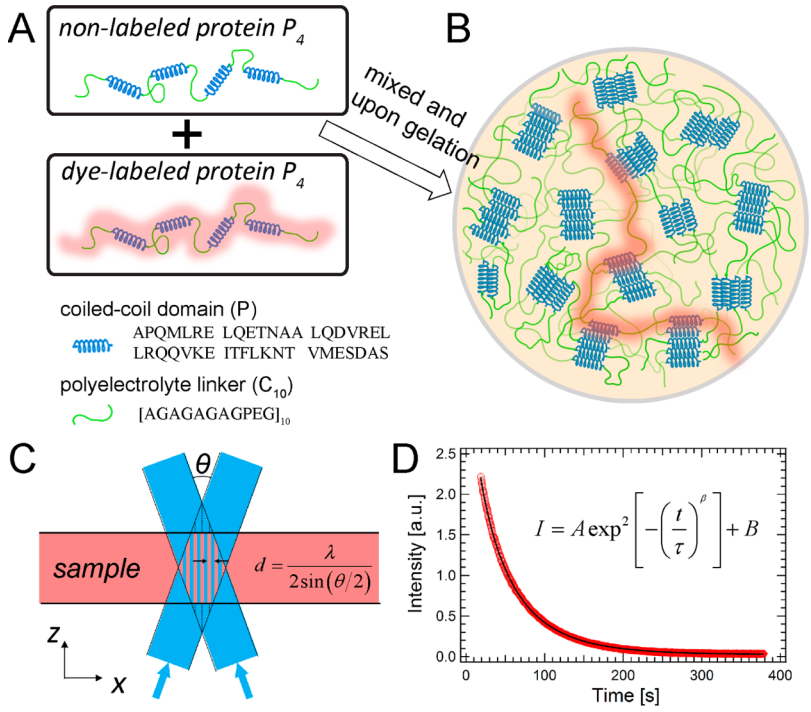

[a](A) Structure of the single protein P_4 that contains four coiled-coil domains on the backbone joined by flexible linkers C_{10}. The chain highlighted in red schematically represents a protein molecule labeled with a single red dye. (B) Schematic of self-diffusion of labeled proteins P_4 in hydrogels made from the same proteins. (C) Forced Rayleigh scattering forms one-dimensional concentration gratings of dye-labeled polymers within a hydrogel when exposed to the full power laser. The blue area within the sample indicates the region of constructive interference, where the photochromic dye was irreversibly isomerized. (D) Diffusion causes decay of the grating. An example showing the decay of the intensity over time (red dots) fit to a stretched exponential function (black line). For this curve, the protein concentration was 10% (w/v) and the measurement was performed at a beam angle of 20° and temperature of 35 °C.

provide exact correlations between the dynamics of one isolated junction and the dynamics of the entire network.[7]

While the majority of existing studies on dynamics have focused on mechanics, diffusion, especially the self-diffusion of network forming molecules, is less explored. However, diffusion is central to understanding the performance of materials and to rationally designing new materials. For example, the diffusion of polymer chains has been shown to affect the structure of the polyelectrolyte multilayers (PEMs) and to further influence their properties.[40] According to the selective phase model,[20,41] diffusion of FG-rich proteins should be critical to promote the translocation through the nuclear pore complex. A similar effect is observed for membrane lipids.[42] Additionally, when cell adhesion epitopes such as RGD are linked to associating polymers inside a synthetic microenvironment, diffusion is expected to alter the spatiotemporal distribution of the cell-binding ligands and thus has an impact on the cell spreading behavior.[31] Diffusion is also relevant for self-healing materials: it is important to know how molecules diffuse across the damaged interface and reform the associative bonds to restore the pristine network structure and mechanical properties.[43] Despite its importance, only a few experimental studies have measured the self-diffusion of polymers in associating networks,[44,45] and this work mainly focuses on diffusion in the large length scale Fickian limit where an effective diffusivity is obtained. Knowledge about how association kinetics quantitatively affect the diffusion of molecules at various length scales is still lacking.

Biosynthetic hydrogels based upon associating coiled-coil domains are an ideal model system for fundamental investigations of gel physical chemistry due to their monodisperse backbone molecular weight and sequence-defined sticker positions. These proteins are widely studied and have also shown promise for a myriad of applications, including artificial extracellular matrices (ECMs),[46−48] biocatalysts,[49,50] and drug carriers.[51] These materials can be modularly designed and engineered by taking advantage of the specificity of coiled-coil association. Here, a multisticker coiled-coil protein is used as model system to study the relationship between associative molecular diffusion and the linear viscoelasticity of gels. The model coiled-coil protein P_4 has a multiblock architecture, with four coiled-coils on the protein backbone joined by flexible polyelectrolyte linkers C_{10} (Scheme 1A,B). For the first time, self-diffusion of associating proteins in hydrogels is measured over four decades of d^2 (square of the diffractive grating spacing) by forced Rayleigh scattering (FRS) (Scheme 1C,D), revealing anomalous diffusion below a critical length scale that largely depends upon temperature and concentration in the gels. Linear viscoelastic properties from 10^{-4} to 10^{2} rad/s are obtained from small-amplitude oscillatory shear (SAOS) and creep measurement, and a sticky Rouse relaxation is first identified in associative protein hydrogels, which correlates to the diffusive motions of associative proteins in an aggregated state. The dissociation rate constants from the diffusion studies provide frequency shift factors, enabling a time−concentration−temperature superposition of the rheology data of gels under various experimental conditions, and collapsed dynamic moduli master curves are obtained. These studies provide quantitative insight into the strong couplings

DOI: 10.1021/jacs.5b00722
J. Am. Chem. Soc. 2015, 137, 3946−3957

between sticker association, molecular diffusion, and material relaxations in associative polymers.

RESULTS AND DISCUSSION

Anomalous Diffusion in Associative Polymers. The self-diffusion of the model associating protein P_4 in hydrogels exhibits two distinct scaling behaviors $\langle\tau\rangle \sim d^{2\mu}$ over a wide range of length scales (Figure 1), where d is the characteristic length scale of the grating and $\langle\tau\rangle$ is the corresponding characteristic diffusion time. It is important to point out that the relation $\langle\tau\rangle \sim d^{2\mu}$ is different than classical scaling of mean square displacement over time ($\langle X^2\rangle \sim t^{\alpha}$), and the two power-law exponents are related by $\alpha = 1/\mu$. At large length scales, an exponent of $\mu = 1$ corresponds to a scaling relation of $\langle\tau\rangle \sim d^2$, as is expected for Fickian diffusion. However, an exponent $\mu < 1$ (or equivalently $\alpha > 1$) is observed at short length scales over a wide range of concentrations, indicating a distance vs time dependence that is stronger than diffusion, i.e., superdiffusion. For example, protein gels at 6.5% (w/v) show a weak power law dependence from ca. 0.05 to 50 μm^2 where the scaling exponent α is 0.304 ± 0.024 (Figure 1). When the concentration of the gel is increased, $\langle\tau\rangle$ increases significantly in the superdiffusive region, from approximately 10 s at a concentration of 6.5% (w/v) to nearly 1000 s at 20% (w/v). The range of d^2 over which the superdiffusive scaling is observed also shifts with increasing concentration; however, the power law exponent α increases only slightly. Previous studies of diffusion in associating polymers were performed on longer length scales corresponding to the effectively Fickian regime observed here;[44,45] this is the first time that superdiffusion is observed through studies of diffusion at shorter length scales. Although this observation may appear counterintuitive at first glance since the presence of associative α-helices reduces the diffusivity of the polymers, the result is reminiscent of the superdiffusion phenomena arising in other self-interacting systems, such as worm-like micelles[52] and *Hydra* cells in aggregates.[53] Although the detailed physics governing these self-interacting systems are substantially different, they share in common that motions of the constituents show spatial and temporal correlations, i.e., movement of one molecule or cell affects the dynamics of others. Therefore, it is hypothesized that the observed superdiffusive scaling regime in associating protein gels originates from the associative dynamics of the coiled-coil domains. However, the scaling exponent μ in the coiled-coil hydrogels is much smaller than the that reported in refs 52 and53 (0.75 and 0.81 for their smallest values, respectively), which suggests a stronger influence of the associative interaction on the diffusion process in the protein gels.

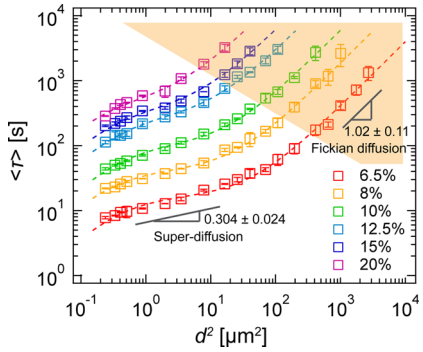

Figure 1. Superdiffusion and Fickian diffusion (shaded in light orange) of coiled-coil proteins in hydrogels at various concentrations. All measurements were performed at 35 °C. Error bars represent one standard deviation of measurements performed in triplicate. Dashed lines are fits to the two-state model. For protein gels at 6.5% (w/v), the values of slopes shown in the figure are from fits to power laws, and error bars on the power law exponents represent 95% confidence intervals.

As the grating spacing is increased into the large d^2 regime, the expected Fickian diffusion is recovered for gels at all concentrations ($\mu = 1.0$). The transition from the superdiffusive regime to the Fickian regime depends on concentration, and the characteristic d^2 at the transition decreases when concentration increases. The corresponding transition length d occurs on the order of μm. Interestingly, there is also a subtle deviation from the superdiffusive scaling in the small d^2 limit where the slope starts to increase, gradually approaching 1.0. This suggests that there might be a second Fickian diffusion regime on very small length scales, where the smallest d in the experiment is still 488 nm, at least an order of magnitude larger than the radius of gyration (R_g) of an individual protein (Supporting Information).

The anomalous diffusion is strongly affected by the temperature (Figure 2). The average decay time constant $\langle\tau\rangle$ at a given grating spacing d^2 increases with decreasing temperature due to the combined effect of a smaller diffusivity of protein molecules and the slower exchange of coiled-coils. In addition, the slope of the power-law regime becomes smaller at

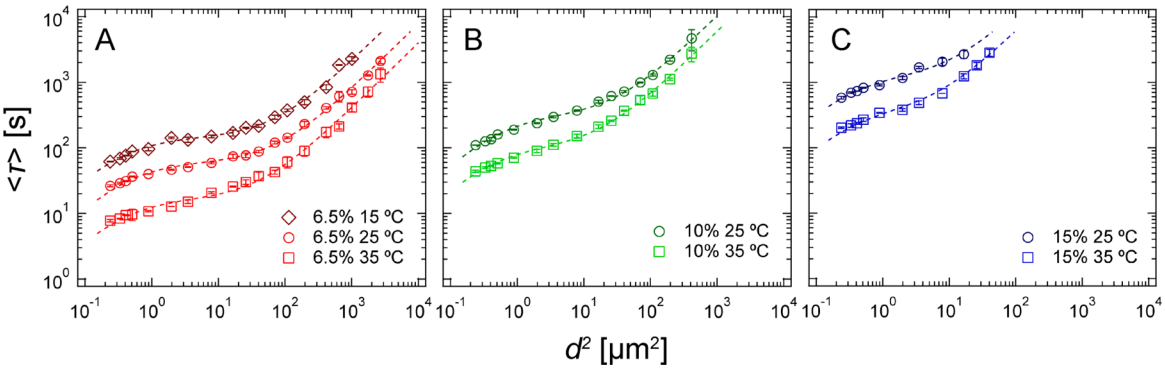

Figure 2. Superdiffusion and Fickian diffusion of coiled-coil proteins in hydrogels at various temperatures. The concentrations in panels (A), (B), and (C) are 6.5%, 10% and 15% (w/v), respectively. Error bars represent standard deviations from measurement in triplicate. Dashed lines are fits to the two-state model.

DOI: 10.1021/jacs.5b00722
J. Am. Chem. Soc. 2015, 137, 3946−3957

lower temperatures; this phenomenon is most pronounced for low concentration gels where both the superdiffusion and Fickian regimes are well developed within the experimentally accessible window. For gels at 6.5% (w/v), the power law exponents are 0.304 ± 0.024, 0.207 ± 0.019, and 0.091 ± 0.078 at 35, 25, and 15 °C, respectively. This observation is consistent with the hypothesis that a smaller μ indicates a stronger association constant for coiled-coils, which is expected with decreasing temperatures.

Analysis of Anomalous Diffusion with the Two-State Model. Previous studies in the literature on associating systems have suggested that the apparent superdiffusive scaling may originate from the interplay of diffusive and associative dynamics.[52,53] In order to quantitatively explore the observed behavior, a two-state model is introduced where a diffusing species is in equilibrium between a molecular state (relatively mobile) and an associated state (relatively immobile). There are two mechanisms by which proteins may diffuse in the associated state: collective motion of clusters of molecules and walking diffusion. In the former mechanism, diffusion of the labeled associated species is achieved by the motion of clusters with a small number of molecules within the larger gel. In the latter case, labeled species diffuse within the associating polymer network by partially detaching the coiled-coil junctions, although at least one coiled-coil along the protein backbone remains attached to the network at all times. Either mechanism can explain the nonzero diffusivity of the associated species. It is also possible that both mechanisms are present; however, the current model cannot distinguish the two. The conversion between states M and A is reversible, and it can be described in the following reaction:

$$M \underset{k_{off}}{\overset{k_{on}}{\rightleftarrows}} A \tag{1}$$

Here, k_{on} and k_{off} characterize the rates at which protein transition between the two states. Changes in the concentrations of protein molecules C_M and C_A can be described simply by the following reaction−diffusion equations, which are referred to as the two-state model hereafter:

$$\frac{\partial C_M}{\partial t} = D_M \frac{\partial^2 C_M}{\partial x^2} - k_{on} C_M + k_{off} C_A$$
$$\frac{\partial C_A}{\partial t} = D_A \frac{\partial^2 C_A}{\partial x^2} + k_{on} C_M - k_{off} C_A \tag{2}$$

where D_M and D_A are the diffusivities in the molecular and associated states, respectively. The model can be solved analytically using Fourier transform methods with the sinusoidal concentration gradients made during the FRS writing step as an initial condition. The initial condition of C_M and C_A can be calculated from the following two relations: $C_A/C_M = K_{eq}$ (from equilibrium assumption) and $C_A + C_M$ = total protein concentration (by definition). The amplitude of the initial sinusoidal concentration profile decays as a double exponential with short and long time constants that are separated by at least 2 orders of magnitude and the small time constant is <1 s even for gels at high concentrations (see details in Supporting Information). Diffracted intensities observed at experimental time scales thus reflect the long relaxation time, which contains effects from diffusion of both molecular and associated species as well as their exchange kinetics, depending on the length scales probed. A similar model has been applied in a study where fluorescence recovery after photobleaching (FRAP) was used to probe the binding interactions and mobility of the transcription factor inside the nucleus, but the diffusivity of the relatively immobile species was assumed to be zero.[54]

Despite its simplicity, the two-state model is able to qualitatively capture many aspects of the experimental observation and provide insight into the underlying physics

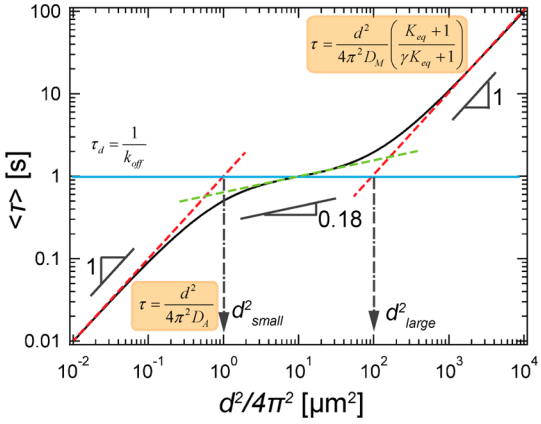

Figure 3. Predicted relation $\langle\tau\rangle \sim d^{2\mu}$ from the two-state model (black solid curve) with the parameter values $D_M = 10^{-8}$ m²/s, $D_A = 10^{-12}$ m²/s, $k_{on} = 100$ s^{-1}, and $k_{off} = 1$ s^{-1}. The solutions (red dashed line) of the two Fickian regimes with slopes of 1 are shown in rounded rectangles with light yellow background. The superdiffusive regime (green dashed line) has a slope of 0.18. The analytical expression for the slope is $2/[1 + (\gamma K_{eq})^{-1/2}]$. The horizontal line in blue corresponds to the molecular dissociation time $\tau_d = 1/k_{off}$.

(Figures 3). In a typical FRS experiment measuring simple Fickian diffusion, the decay time of the diffracted intensity is

$$\tau = \frac{d^2}{4\pi^2 D} \tag{3}$$

where D is the diffusion constant of the dye-labeled species, and d is the period of the holographic grating defined by following equation (Scheme 1C):

$$d = \frac{\lambda}{2\sin(\theta/2)} \tag{4}$$

In this two-state model, the relationship between the observed time constant and diffusivity is significantly more complex. As shown in Figure 3, the model predicts the existence of two Fickian regimes at both large and small d^2 with slopes of one in the log−log plot. They are connected by a pseudo power-law regime with a slope <1, which indicates superdiffusion.

These regimes can be explained by considering the physical processes that govern the relaxation of the imposed concentration gradient in the FRS experiment, which can include the diffusion of molecules in both molecular and associated states, and the exchange kinetics between the two states. In all regimes, complete relaxation is only possible after the concentration gradient of the relatively immobile associated proteins has relaxed. At the shortest length scales, the diffusion time scale of associated molecules is sufficiently short that the gradient can relax directly by diffusion, thus

$$\tau = \frac{d^2}{4\pi^2 D_A} \tag{5}$$

DOI: 10.1021/jacs.5b00722
J. Am. Chem. Soc. 2015, 137, 3946−3957

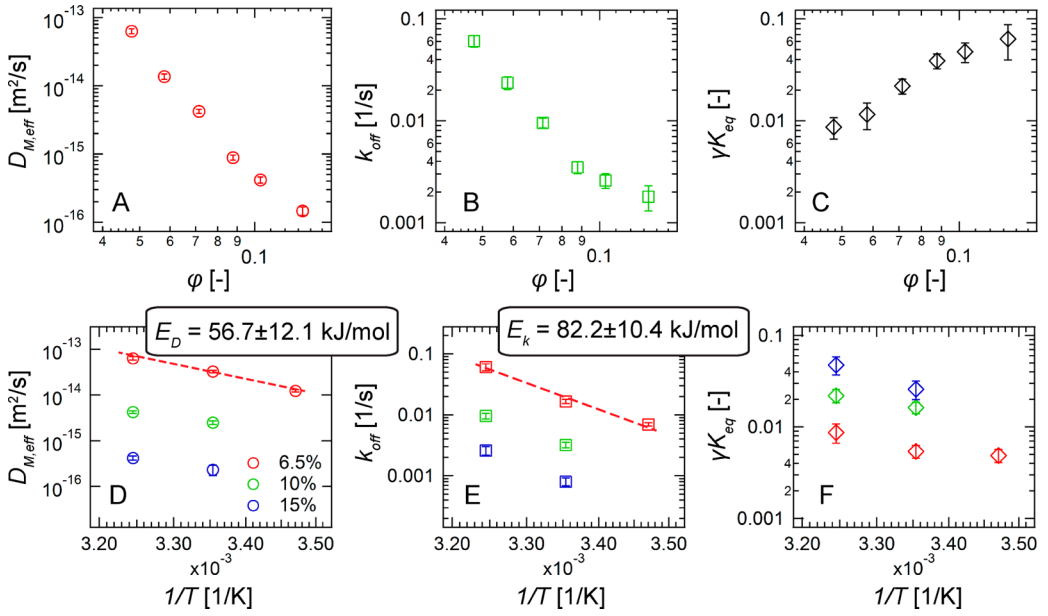

Figure 4. Estimated diffusivities $D_{M,eff}$, and rate constant k_{off}, and γK_{eq} as functions of the volume fraction of protein φ (A–C) and the inverse of temperature (D–F). Error bars represent 95% confidence intervals from fits to the two-state model. The values of estimated activation energies are shown in the text box on top of the corresponding panel.

At the longest length scales, the most rapid relaxation pathway is for proteins to disconnect from the network and diffuse as individual molecules. Therefore, the predicted relaxation time reflects the diffusion of free molecules, slowed down by continuous association/disassociation with the network. The resulting grating relaxation time is

$$\tau = \frac{d^2}{4\pi^2 D_M}\frac{K_{eq}+1}{\gamma K_{eq}+1} \tag{6}$$

Since the association energy between the coiled-coil domains is large relative to k_BT,[55] it is expected that the association rate is much larger than the dissociation rate, i.e., $k_{on} \gg k_{off}$, or the equilibrium constant ($K_{eq} = k_{on}/k_{off}$) is large. In the limit when the ratio of associated diffusivity to molecular diffusivity ($\gamma = D_A/D_M$) is small enough such that $\gamma K_{eq} \ll 1$, the grating relaxation time in the Fickian regime at large d^2 simplifies to

$$\tau = \frac{d^2}{4\pi^2 D_M}K_{eq} \approx \frac{d^2}{4\pi^2 D_{M,eff}} \tag{7}$$

where the effective diffusivity turns out to be the real diffusivity D_M divided by the equilibrium constant K_{eq}. In the strong association limit, the equilibrium constant should be the inverse of the fraction of dissociated chains (f),

$$K_{eq} = \frac{k_{on}}{k_{off}} = \frac{C_{A,eq}}{C_{M,eq}} = \frac{1-f}{f} \approx \frac{1}{f} \tag{8}$$

Therefore, the effective diffusivity can also be expressed as

$$D_{M,eff} = \frac{D_M}{K_{eq}} = fD_M \tag{9}$$

which is the bare diffusivity of the molecular species multiplied by the fraction of dissociated chains. At intermediate lengths, diffusion in the molecular state is still the dominant mechanism, but the grating relaxation time is determined by the conversion rate from the associated state to the molecular state, i.e., k_{off}.

The emergence of the superdiffusive regime can also be explained from a time-scale perspective. The superdiffusive regime is centered around the molecular "off" time, $\tau_d = 1/k_{off}$, which provides a characteristic time scale for proteins to dissociate from the network. For a time period much shorter than τ_d, the dissociation effect is negligible on the time scale over which the grating decays. Therefore, the decay of the FRS grating is due to the diffusive motion of the more abundant but less mobile associated molecules (eq 5). By comparison, for a time period much longer than τ_d, protein molecules dissociate and reassociate with the network several times during the characteristic decay time. The molecules are able to diffuse after disconnecting from the network following Fick's law, but they spend a significant fraction of time associated with the surrounding proteins that effectively slows down the diffusion. Therefore, hindered diffusion of relatively mobile protein molecules is observed (eqs 6–9). The superdiffusive regime arises from the transition between the two Fickian limits, where the association/dissociation dynamics is important. In this regime, the rate of grating decay is limited by the rate of network dissociation, not by the size of the grating. Because most of the coiled-coils have formed pentameric aggregates with each other in the strong association limit and are not available for free molecules to bind, molecules can diffuse a distance larger than the grating period before reassociating with the network. Hence the rate-limiting step is the dissociation of protein molecules and the averaged time constant centers around τ_d. Last, it should be emphasized that a nonzero value of γ or D_A is required to yield a nonzero slope in the power-law region and to observe the Fickian regime at small length scales. This is a critical difference between the analysis presented here and previous formulations of the two-state model where the diffusion of relatively immobile species is neglected.[54]

Fitting the two-state model to experimental data provides quantitative estimates of the rate constants and diffusivities of the two species. While the model does not presuppose any values for the diffusivities or rate constants, the regime relevant to associating polymer gels has $K_{eq} \gg 1$ due to strong

DOI: 10.1021/jacs.5b00722
J. Am. Chem. Soc. 2015, 137, 3946–3957

association of the physical bonds and $\gamma \ll 1$ arising from a fast and slow species. Fitting is restricted to this regime to obtain physically relevant solutions; within this regime super diffusive behavior emerges when $\gamma K_{eq} \ll 1$. Because the model predicts that all curves collapse under the experimentally relevant condition when $K_{eq} \gg 1$ and $\gamma K_{eq} \ll 1$ (Supporting Information), only three parameters can be independently determined without imposing a specified value of K_{eq}, which are chosen to be the off-rate constant k_{off}, the diffusion coefficient of associated species D_A, and the quantity γK_{eq}. As shown in Figures 1 and 2, the two-state model is able to fit the experimental data with satisfactory agreement under all conditions of temperature and concentration. With the assumption that $K_{eq} \gg 1$ and $\gamma K_{eq} \ll 1$, the effective molecular diffusivity $D_{M,eff}$ simplifies to D_M/K_{eq} and can be calculated from $D_A/\gamma K_{eq}$. As shown in Figure 4A,D, $D_{M,eff}$ is estimated to be in the range of 10^{-16}–10^{-13} m^2/s, at least 2 orders of magnitude smaller than the self-diffusion coefficients of typical polymers in the semidilute regime.[56,57] This observation supports the argument that the association between protein molecules effectively slows down the rate of diffusion. The value of D_A falls into the range of 10^{-18}–10^{-16} m^2/s (Figure S5 in Supporting Information). It is much smaller than D_M given that $K_{eq} \gg 1$, but is not negligible. k_{off} has values ranging from 0.1 to 0.001 s^{-1}, and its inverse falls into the time scale in the FRS experiments.

The estimated reaction–diffusion parameters allow quantitative comparisons between observations under different experimental conditions. First, the diffusion coefficients decrease with increasing concentration (Figure 4A and S6 in Supporting Information), as expected. The concentration dependencies are appreciably stronger than what has been reported in literature,[58] but the scaling $D_{M,eff} \sim \varphi^{-5.96\pm0.96}$ and $D_A \sim \varphi^{-3.88\pm0.68}$ (error bars represent 95% confidence of intervals) are qualitatively consistent with the sticky Rouse predictions.[35] The rate constant k_{off} decreases with increasing concentration (Figure 4B), indicating that k_{off} is fundamentally different than the rate constant in classic biomolecular reactions, which is a function of temperature only. Even though a single coiled-coil could break at a rate independent of concentration, dissociation of a protein molecule, which requires collective dissociation of four coiled-coil domains, may exhibit concentration dependence, possibly due to differences in the fraction of dissociated coiled-coil domains and/or chain connectivity (loops vs bridges). At equilibrium, the fraction of dissociated coiled-coils decreases with concentration. Therefore, the collective rate for all four coiled-coil domains dissociating from an individual protein goes down. In addition, previous work has demonstrated that the fraction of bridged chains increases with concentration.[30] Dissociation of a bridged chain should be relatively more difficult than a looped chain because it causes changes in the association states of the stickers (closed or open) not only on the bridged chain but also on others connected by intermolecular coiled-coil aggregates. Collectively, it is reasoned that a chain undergoes many failed attempts to disengage from the network before a successful dissociation event takes place. This phenomenon leads to a smaller k_{off} at higher concentrations. The observed concentration-dependent dissociation rate, or dissociation time, is also in agreement with the concept of bond lifetime renormalization in the sticky Rouse theory.[35]

Both diffusivities and k_{off} increase with temperature as a result of enhanced thermal fluctuations, and they follow an empirical Arrhenius behavior over the relatively limited experimental temperature range (Figure 4D,E, and Figure S6 in Supporting Information). The Arrhenius behavior is possibly due to energy barriers required for proteins to dissociate from the network, not the free volume effect in self-diffusion of an unentangled polymer melt.[59] Temperature has a more profound effect on dissociation kinetics than the effective molecular diffusivity, as the activation energy of $D_{M,eff}$ (56.7 ± 12.1 kJ/mol) is smaller than the one of k_{off} (82.2 ± 10.4 kJ/mol). The activation energy of D_A, however, is roughly the same as for k_{off} within statistical error (Supporting Information), suggesting that D_A/k_{off} might be temperature insensitive. The quantity D_A/k_{off} is proportional to the transition d^2 from the small-length-scale Fickian regime to the superdiffusive regime, which can be obtained by setting $\tau = 1/k_{off}$ in eq 5:

$$d^2_{small} = \frac{4\pi^2 D_A}{k_{off}} \tag{10}$$

However, the reason why d^2_{small} does not depend on temperature remains to be determined.

Finally, the product γK_{eq} quantitatively describes the extent of anomalous diffusion, because it is the combined ratio of the two diffusion coefficients and the two rate constants. The nondimensionalized average time constant and square of the grating spacing are defined as $\tilde{\tau} = k_{off}\langle\tau\rangle$ and $\tilde{d}^2 = k_{off}\, d^2/4\pi^2 D_{M,eff}$ (or equivalently $\gamma K_{eq} k_{off}\, d^2/4\pi^2 D_A$), respectively, where the symbol ~ indicates dimensionless variables. Figure 5 shows that all curves collapse in the Fickian regime at large d^2,

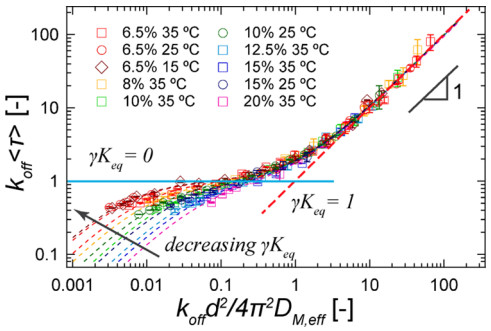

Figure 5. Anomalous diffusion plotted in reduced parameter space. The dotted lines are normalized fits to the two-state model. The red dashed line represents the reduced asymptotic solution in the large d^2 Fickian regime. The navy blue line represents the limiting case where $\gamma K_{eq} = 0$.

and the reduced solution in this regime becomes simply $\tilde{\tau} = \tilde{d}^2$. If $\gamma K_{eq} = 1$, this Fickian regime continues to the smallest the length scale until subdiffusive motions of polymer segments have to be considered. For all the cases in the current study, where $\gamma K_{eq} \ll 1$ (Figure 4C,F), a superdiffusion regime starts to develop when $\tilde{d}^2$ or $\tilde{\tau}$ decreases to one. The width of the superdiffusive regime w is defined as the ratios of the two d^2 from the line $1/k_{off}$ intersecting the two Fickian solutions (Figure 3):

$$w = \frac{d^2_{large}}{d^2_{small}} = \frac{4\pi^2 D_M/(K_{eq} k_{off})}{4\pi^2 D_A/k_{off}} = \frac{1}{\gamma K_{eq}} \tag{11}$$

DOI: 10.1021/jacs.5b00722
J. Am. Chem. Soc. 2015, 137, 3946–3957

Therefore, w increases with decreasing γK_{eq}, as observed for gels at low concentrations or at low temperatures (Figures 1, 2, and 5). As shown in the Supporting Information, the slope of the superdiffusive regime is

$$\left.\frac{d\log \tau}{d\log d^2}\right|_{\text{inflection}} \approx \frac{2}{1+\sqrt{w}} = \frac{2}{1+(\gamma K_{eq})^{-1/2}} \quad (12)$$

which is also a function of γK_{eq} only. When γK_{eq} is nonzero, the slope or the power-law exponent can take any value from zero to one. From eq 12, it is clear that a smaller value of γK_{eq} yields a smaller slope in the superdiffusive regime (Figures 1, 2, and 5). In the limiting case where $\gamma K_{eq} = 0$, when either associated species are completely immobile or the reassociation rate is zero, the superdiffusive regime with a slope of zero is predicted to persist to the smallest length scale. However, for nonzero γK_{eq}, all curves enter a second Fickian regime below the length scale of the superdiffusive regime, where the reduced solution is $\tilde{\tau} = (\tilde{d}^2/\gamma K_{eq})$. Therefore, the dimensionless transition $\tilde{d}^2$ from the power-law regime to this small-length-scale Fickian regime is γK_{eq}, from 0.004 to 0.06 in the experiment, as shown in the collapsed data in Figure 5. It is important to point out that both Fickian regimes cannot be superimposed simultaneously because curves with different values of γK_{eq} have different shapes. If $\tilde{d}^2$ is defined as $k_{off}\, d^2/4\pi^2 D_A$, the curves will instead collapse in the small-length-scale Fickian regime.

The Rheological Signature of Sticky Rouse Relaxation in Protein Gels. Shear rheology is performed in order to study the relationship between the dynamics on the molecular level measured by self-diffusion and a material's macroscopic relaxation. Dynamic moduli master curves are obtained in the frequency range from 10^{-4} to 10^{2} rad/s by combining creep and frequency sweep measurements (Supporting Information). As shown in Figure 6A, P_4 hydrogels exhibit a plateau storage modulus G'_∞ in the high-frequency regime (10−100 rad/s), and a crossover between G' and G'' at intermediate frequencies (0.1−1 rad/s) where the relaxation time of the coiled-coil domains can be assigned; both features are typically observed for physical hydrogels. In addition, a noticeable turn in G' is present in the frequency regime 0.001−0.01 rad/s before entering the terminal relaxation regime. Corresponding to this turn in G', there exists a second plateau in the relaxation modulus master curve (Figure 6B) and a local minimum in the van Gurp−Palmen plot (Figure S7 in Supporting Information). The existence of an additional relaxation in this low frequency range resembles the rheological responses from a variety of systems where the sticky Rouse theory can be applied, such as ionomers,[60,61] hydrogen-bond polymers,[62] and small molecules;[63] but to the best of our knowledge, this has not been reported or thoroughly investigated in previous studies on gels. More importantly, this sticky Rouse relaxation can be observed in protein gels formed by the same coiled-coil domain but with different number of stickers or with different molecular architecture (multiblock vs triblock) (Figure S8 in Supporting Information). The finding here agrees with a theoretical study from Indei et al. that the sticky Rouse relaxation is universal in transient networks formed by associating polymers.[64]

In the high-frequency regime, despite precisely defined molar mass and spacing between stickers, the coiled-coil protein gels still show a broad relaxation distribution corresponding to network junction relaxation. In these protein gels, the relaxation process over the range from 0.1 to 100 rad/s is broader than predicted by the Maxwell model (Figure S9 in Supporting Information), similar to phenomena observed in other physical gels.[31,65,66] A better fit is obtained using the Kohlrausch−Williams−Watts (KWW) model (Figure 6, see model description in Supporting Information). A stretched exponent β of 0.620 ± 0.003 is obtained, which suggests significant inhomogeneity in the relaxation process. Traditionally, the origin of this broader-than-Maxwell relaxation has been attributed to the molecular weight distribution of polymers/proteins, the non-uniform distribution of stickers, and possible effects from chain entanglement. In the coiled-coil protein hydrogel systems studied here, all of these plausible explanations can be ruled out since the protein is strictly monodisperse, the locations of the coiled-coil domains are precisely controlled, and the concentration is below the entanglement threshold.[30] Therefore, the dispersity of the relaxation modes is hypothesized to originate from other forms of dynamic heterogeneity.

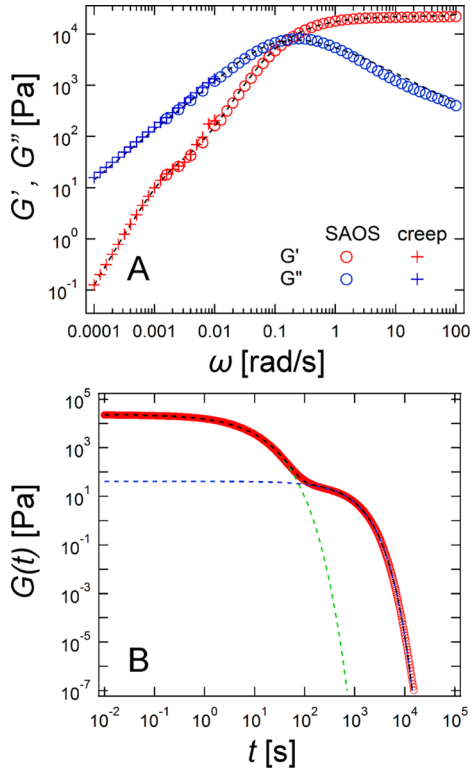

Figure 6. Representative dynamic moduli master curves (A) and relaxation modulus master curve (B) of protein gels at 25% (w/v) measured at 25 °C. Black dashed lines in figures represent the fit to a sum of two KWW functions. The green and the blue dashed lines in (B) illustrate the contribution of relaxation modulus from the fast mode and the slow mode relaxations, respectively.

The low-frequency rheological response can be fit by the sticky Rouse or the KWW models, although the empirical KWW model can provide a quantitative fit in the absence of specific information on the configuration of the proteins in solution. The sticky Rouse model is used to describe the dynamics of polymers with associating side groups below the entanglement threshold.[34−36] It was first proposed by Rubinstein, Semenov, Leibler, and Colby and has recently found great success in modeling the dynamics of ionomers.[60,61] This model reasons that the relaxation motions of chains larger than the size of a sticky Rouse segment can be constrained by the association of the stickers, whereas the Rouse modes are

DOI: 10.1021/jacs.5b00722
J. Am. Chem. Soc. 2015, 137, 3946−3957

unaffected for segments with sizes smaller than the chains between stickers. Hence the relaxation modulus has contributions from the normal Rouse modes (high order modes, $p > N_s$) and the sticky Rouse modes (low order modes, $p \leq N_s$):[60]

$$G(t) = \frac{\rho\varphi RT}{M}\left[\sum_{p=N_s+1}^{N} \exp\left(-\frac{tp^2}{\tau_0 N^2}\right) + \sum_{p=1}^{N_s} \exp\left(-\frac{tp^2}{\tau_s N_s^2}\right)\right] \quad (13)$$

where τ_0 is the relaxation time of the Rouse segment, τ_s is the relaxation time of the sticky segment, N is the number of Rouse segments in the chain, and N_s is the number of sticky Rouse segments in the chain. However, due to the difficulty in experimentally determining τ_0 and τ_s of coiled-coil proteins, rheology data in this frequency regime is fit to the phenomenological KWW function, and a satisfactory fit is obtained (Figure 6). The stretched exponent in this regime is 0.868 ± 0.003, indicating that the distribution of relaxation modes in this regime is smaller than the one in the high-frequency domain, but it does show some extent of dispersity in the relaxation modes. However, the origin of the less inhomogeneous relaxation in the low-frequency range is not well understood.

Taken together, the relaxation of associative protein gels over the frequencies range from 10^{-4} to 10^{2} rad/s can be described by a sum of two KWW functions:

$$G(t) = G_C \exp\left[-\left(\frac{t}{\tau_{KWW,C}}\right)^{\beta_C}\right] + G_{SR} \exp\left[-\left(\frac{t}{\tau_{KWW,SR}}\right)^{\beta_{SR}}\right] \quad (14)$$

where the subscripts C and SR denote the contribution from the coiled-coil exchange dynamics and from the sticky Rouse relaxation, respectively. Although this approach is entirely based on empirical models, it only uses six parameters and is able to capture most of the important features in the rheology data over six decades. This approach can be applied for gels at all investigated concentrations (Figure 7).

Collapsed Shear Rheology Master Curve. The dissociation rate of the coiled-coil domains in rheology directly correlates with the dissociation rate of protein molecules from diffusion measurements, which provides the fundamental basis for a time−concentration−temperature superposition in the rheology data over a certain concentration regime. Many previous studies have suggested that the relaxation of transient networks is primarily governed by the dissociation rate of stickers.[7,62,67,68] In particular, a seminal study from Craig and co-workers[7] demonstrates that the rheological behavior is self-similar for various physical networks based upon different metal−ligand coordination bonds, and a flow master curve $\eta k_d \sim \omega/k_d$ can be obtained by using molecular dissociation constant k_d as the scaling parameter.[7] However, for systems where the network junctions have a functionality >2, the dissociation dynamics used by Craig to rescale the rheological response cannot be clearly defined or be easily measured. In addition, it remains unclear whether Craig's approach can be applied to various concentration regimes under the sticky Rouse framework. A recent study on low-concentration physical gels argues that the Arrhenius factor, not the dissociation rate, is the correct frequency scaling factor to obtain collapsed rheology curves.[69] Here, the average time constant from the KWW function at higher frequencies:

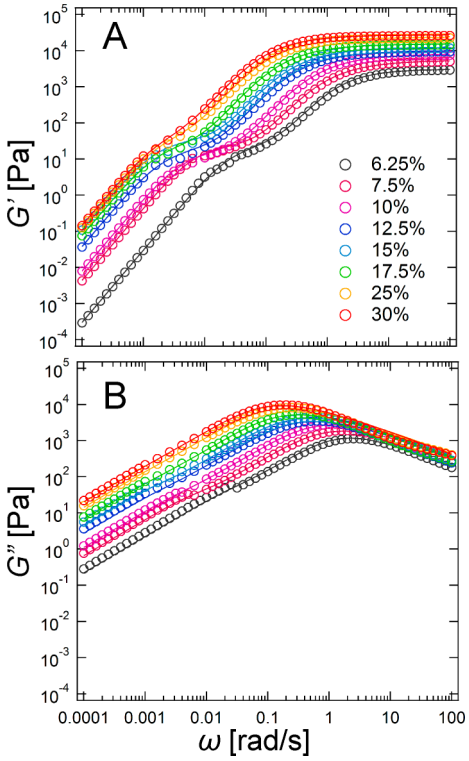

Figure 7. Dynamic shear moduli master curves of unentangled multiblock coiled-coil protein hydrogels at various concentrations (G' in panel A, and G'' in panel B). Experimental data are plotted in open circles, and the solid lines are fits to eq 14.

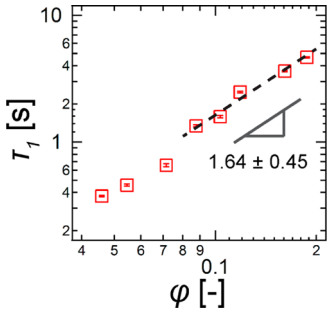

Figure 8. Concentration dependence of the time constant τ_1 from the KWW function at high frequencies. Error bars represent 95% confidence interval from fits to the KWW function. Only the concentration range for φ = 0.088 (corresponding to 12.5% w/v) and above is fitted because intermolecular coiled-coil association dominates in this range.

$$\tau_1 = \frac{\tau_{KWW,C}}{\beta_C}\Gamma\left(\frac{1}{\beta_C}\right) \quad (15)$$

is assigned to be the hydrogel relaxation time (Γ is the gamma function), and its concentration dependence is plotted in Figure 8. A scaling relation $\tau_1 \sim \varphi^{1.64\pm0.45}$ is observed for gels at φ = 0.088 (corresponding to 12.5% w/v) and above, and the scaling exponent is close to the one in $\tau_d \sim \varphi^{1.57\pm1.26}$ ($\tau_d = 1/k_{off}$; and the relatively large error bar is due to a limited concentration range accessible in diffusion measurements). This suggests that τ_1 and τ_d might both originate from the dissociation of coiled-coil domains. However, τ_1 and τ_d are essentially different: τ_d describes the dissociation time of protein molecules from networks that demands simultaneous

DOI: 10.1021/jacs.5b00722
J. Am. Chem. Soc. 2015, 137, 3946−3957

disengagement of all coiled-coil domains on a single chain, whereas τ_1 is the time of network relaxation, which only requires exchange between some of the coiled-coils that relaxes elastically effective midblock segments. Thus, it is not surprising that τ_d measured by diffusion is on the order of 1000 s, which is 2 to 3 orders of magnitude larger than the segmental relaxation time τ_1 measured by rheology (Figure S10 in Supporting Information).

Nonetheless, because of the common molecular origin of both processes, the dissociation rate constant k_{off} from diffusion studies can be utilized to produce dynamic moduli master curves by defining a reduced angular frequency as $\tilde{\omega} = \omega/k_{off}$ (i.e., the shift factor is $1/k_{off}$) and reduced moduli as $\tilde{G}' = G'/G'_{max}$ and $\tilde{G}'' = G''/G'_{max}$, where G'_{max} is the high-frequency plateau modulus at that particular concentration. Rate constants k_{off} not measured at the reference temperature (25 °C) are calculated from the concentration scaling $k_{off} \sim \varphi^{-1.57}$ and the Arrhenius law $\ln k \sim E/RT$. As shown in Figure 9, the rheology

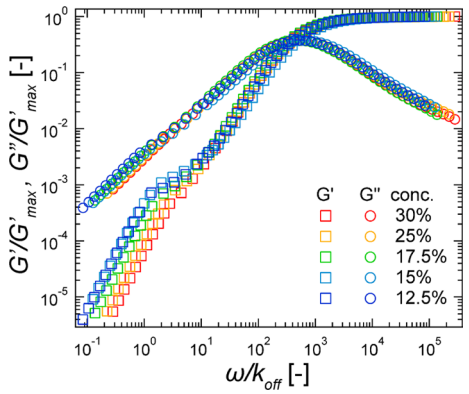

Figure 9. Rheology data plotted in the reduced parameter space. The parts in the high-frequency regime collapse onto a single curve. The reference temperature is at 25 °C.

data from gels at 12.5% (w/v) and above collapse at reduced frequencies from 10^6 to 10. Furthermore, the onset of the terminal regime appears where the reduced frequency is of order one. This suggests that sticky protein molecules are able to "freely" diffuse for times longer than $1/k_{off}$, consistent with the definition of the terminal regime. While similar results have been reported,[44] previously findings and conclusions were confounded by the effect of structural polydispersity, which is absent in the protein gels studied here. Since the method considers the effect of both concentration and temperature on the relaxation dynamics, it is termed time−concentration−temperature superposition. By examining the concentration dependence of the zero-shear-rate viscosity η_0 (Figure S11 in Supporting Information), the concentration range in the rheological study may be divided into two regimes: the low concentration regime below $\varphi = 0.071$ (i.e., 10% w/v) and the high concentration regime above $\varphi = 0.088$ (i.e., 12.5% w/v), where the number fraction of elastically effective chains is 0.68 and above under the affine network assumption (Figure S12 in Supporting Information). The scaling $\eta_0 \sim \varphi^{2.46}$ also shows qualitative agreement with the prediction from the sticky Rouse theory.[35] Note that the highest concentration 30% (w/v) is still below the threshold at which strands between two adjacent stickers overlap.[30] Therefore, the superposition of rheology data demonstrates that the network relaxation is indeed controlled by the dissociation rate of stickers. In addition, the superposition method applies when the concentration lies in the regime $\varphi_{ren} < \varphi < \varphi_s$, i.e., the concentration is high enough such that the intermolecular association dominates and bond lifetime renormalization should be considered ($\varphi_{ren} < \varphi$), but it is still below the overlap concentration of sticky Rouse segments (φ_s). It is important to point out that gels investigated in the seminal work from Craig also fall into the regime $\varphi_{ren} < \varphi < \varphi_s$ (see analysis in Supporting Information). Finally, it is observed that the rheology data start to diverge below a reduced frequency of 10 due to the sticky-Rouse-like relaxation, in agreement with previous studies on ionomers.[60]

The sticky Rouse signature in the rheology data is hypothesized to originate from the collective motion of associative protein molecules in an aggregated state because of the high valency of coiled-coil junctions. It is important to emphasize that the gels are clear, showing no signs of macrophase separation, and that this motion of associated species cannot be correlated to a structural length scale within the gel. While the sticky Rouse model cannot be readily applied to quantitatively describe the rheological behavior of protein hydrogels, it provides an estimate of the size of a "dynamic relaxation unit". By setting $t = 0$ in eq 13, the sticky Rouse model gives a molecular weight−modulus relationship:

$$G_{SR} = \frac{\rho\varphi RT}{M}N = \frac{\rho\varphi RT}{M_{eff}} \tag{16}$$

where M_{eff} is the effective molecular weight of a "relaxation unit" on the long time scale, ρ is the density of proteins (estimated to be 1.30 from previous work),[30] and G_{SR} is the sticky Rouse modulus in eq 13, whose value is obtained by fitting to the KWW model. Thus, the number of protein molecules in a relaxation unit θ is calculated to be

$$\theta = \frac{M_{eff}}{M_0} = \frac{\rho\varphi RT}{G_{SR}M_0} \tag{17}$$

where M_0 is the molecular weight of a single protein P_4 (62.8 kDa). Figure 10 depicts the concentration dependence of G_{SR}

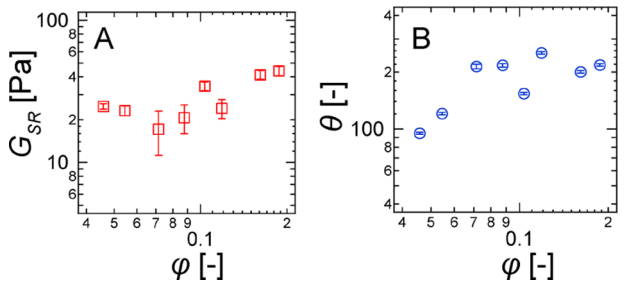

Figure 10. Concentration dependence of (A) the sticky Rouse relaxation modulus G_{SR} and (B) the number of proteins in a "dynamic relaxation unit" θ. Error bars represent 95% confidence intervals.

and θ. Because the sticky Rouse modulus G_{SR} has a value of 20−45 Pa, θ is calculated to be in the range of 100−200. The large number suggests that the relaxation unit could be aggregated proteins originating from thermal fluctuation or dynamic heterogeneity within the transient network. This is a key difference between the protein gels studied here and other associating physical networks where the sticky Rouse rheological feature comes from the hindered motion of polymer chains;[60−62] but it is reminiscent of observation of the supramolecular structure in hydrogen-bonded monohydroxy

DOI: 10.1021/jacs.5b00722
J. Am. Chem. Soc. 2015, 137, 3946−3957

alcohols where the sticky-Rouse-like relaxation is due to dynamic molecular aggregation.[63]

CONCLUSIONS

Unexpected anomalous self-diffusion is observed in associating polymer gels for the first time using a model system of associating coiled-coil protein hydrogels. On time scales approximately equal to the molecular dissociation time, superdiffusion is shown, which originates from the interplay between association dynamics and diffusion of proteins in an unbound state and an associated state. On large time scales, Fickian diffusion is recovered but is effectively slowed by the fraction of dissociated chains in the strong association limit. The observed anomalous behavior can be quantitatively explained by a simple two-state model that accounts for dynamic exchange of molecules between a free molecular state and an associated state, providing estimates on the diffusivities and the rate constants. Importantly, even in the associated state, molecules still have a small but nonzero diffusivity. Hindered diffusion of associating proteins in molecular and aggregated states also manifests in the shear rheology master curves, which displays sticky-Rouse-like relaxation at low frequencies. It is shown that high-frequency relaxation of the model transient network is primarily controlled by the dissociation rate of stickers, but the principle of time−concentration superposition only holds in a concentration regime where the intermolecular association becomes dominant. The concentration scaling relations of diffusivities and the zero-shear-rate viscosity and the concentration-dependent dissociation rate are qualitatively consistent with the sticky Rouse theory.

EXPERIMENTAL METHODS

Protein Synthesis and Purification. The genes encoding for associating protein P_4 and P_4-Cys have been previously reported, and the full expressed protein sequences are available in the literature.[70,71] Both proteins have four coiled-coils on the protein backbone joined by flexible polyelectrolyte linkers C_{10}, and the protein P_4-Cys has a single cysteine residue near the C terminus that enables efficient labeling with maleimide-functionalized dye molecules (Scheme 2). The

Scheme 2. Efficient Synthesis of ONS-Labeled Proteins P_4 via Thiol-Maleimide Conjugation

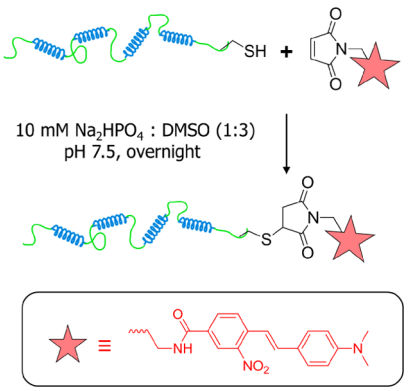

detailed procedure for protein synthesis and purification has been reported in previous work.[30,72] Briefly, proteins were expressed in *Escherichia coli* and purified by ammonium sulfate precipitation and anion exchange chromatography using HiTrapQ Sepharose HP 5 mL columns. Combined pure fractions (determined by SDS-PAGE) were dialyzed against Milli-Q water extensively and lyophilized.

Synthesis and Purification of *ortho*-Nitrostilbene (ONS)-Labeled Proteins P_4. The synthesis of the maleimide-functionalized photochromic 4′-(*N*,*N*′-dimethylamino)-2-nitrostilbene dye (ONS-M) followed a previously published procedure.[73] In a typical conjugation reaction (Scheme 2), protein P_4-Cys was first dissolved in a 3:1 (v/v) mixture of DMSO: (10 mM NaH_2PO_4) to a concentration of 1 mg/mL, and the solution was stirred at room temperature for 2 h to ensure complete dissolution of proteins. Next, a 20-fold excess of tris(2-carboxyethyl)phosphine (TCEP) and ONS-M relative to the cysteine residue was added, and the pH of the reaction mixture was adjusted to 7.5. After overnight reaction in the dark, the mixture was dialyzed against Milli-Q water and lyophilized. To remove the unreacted free dye, the lyophilized powder was redissolved in a buffer with 6 M urea and 20 mM Tris at pH 8.0 (freshly prepared). The product was first purified by anion exchange using HiTrapQ Sepharose HP 5 mL columns (GE Healthcare) and further purified by size exclusion with Sephadex LH-20 resins (GE healthcare). The conjugation efficiency was >99% confirmed by UV−vis spectroscopy.

Forced Rayleigh Scattering (FRS) Measurements. The protein gels for diffusion measurement were prepared by hydrating ONS-labeled P_4 and matrix P_4 in 100 mM sodium phosphate buffer at pH 7.6 to the desired concentrations at 4 °C for 2 days, and the concentration of ONS-P_4 was approximately at 150 μM. The gels were mixed periodically to ensure homogeneous distribution of dye-labeled proteins and then pressed in between two quartz disks (0.9 in. in diameter) with a 0.5 mm Teflon spacer in a brass sample holder. The specimens were annealed at 37 °C for 2 h in the dark to eliminate shear history from loading. Samples were equilibrated at the desired experimental temperature for at least 1 h before measurement. Diffusion was measured by FRS, a technique widely used in probing slow diffusion of molecules in colloids, micelles, and self-assembled block copolymers.[74,75] Compared to other popular methods of studying diffusion, such as FRAP, FRS has the advantage of accessing length scales close to the diffraction limit while measuring over time scales comparable to FRAP.[74] FRS measurements were performed as previously described.[73,76] Briefly, a 100 mW continuous wave laser operating in single longitudinal mode at λ = 488 nm was split into two beams, which were individually refocused and crossed at an angle of θ onto the sample (Scheme 1C). This generated a holographic grating of characteristic spacing d that is determined by eq 4. By exposing the sample for 250 ms, the photochromic ONS dye was irreversibly isomerized in the areas of constructive interference, resulting in an amplitude grating of dye concentration. The evolution of the resulting sinusoidal concentration profile by diffusion was monitored by diffraction of a single reading beam at the same wavelength and angle as one of the writing beams, but attenuated by 10^{-5}. The intensity of the reading beam was low enough such that the change of the profile was due only to diffusion. After a fast initial decay in the intensity with a time constant 2 orders of magnitude smaller than the time constant for the long decay (Figure S1 and Supporting Information), the signal was fit to a stretched exponential function:

$$I = A\ \exp^2\left[-\left(\frac{t}{\tau}\right)^{\beta}\right] + B \tag{18}$$

where I is the intensity, τ is the time constant, β is the stretched exponent ranging from 0 to 1, and B is the incoherent background. Only the slow decay with a larger time constant was considered (Supporting Information). The average decay time constant was calculated as the first moment of the stretched exponential:

$$\langle\tau\rangle = \frac{\tau_{KWW}}{\beta}\Gamma\left(\frac{1}{\beta}\right) \tag{19}$$

where Γ is the gamma function.

Rheology Experiments and Data Analysis. Lyophilized proteins were hydrated in 100 mM sodium phosphate buffer (pH 7.6, filtered through 0.2 μm PES filters) to the specified concentrations. Hydrogel samples were kept at 4 °C for 2 days to allow complete hydration. Linear rheological measurements of protein

DOI: 10.1021/jacs.5b00722
J. Am. Chem. Soc. 2015, 137, 3946−3957

hydrogels were performed on Anton Paar MCR 301 and MCR 702 rheometers. For consistency, motor adjustment and inertial calibration were performed before each experiment. A cone and plate geometry (25 mm, 1° cone) was used for all samples, and a larger cone (50 mm, 0.5°) was used to perform measurements at low torques. Hydrogel samples were coated at the edge with mineral oil to minimize dehydration. The effect of low-viscosity mineral oil on the rheological measurements was negligible as the torque generated from oil was over 3 orders of magnitude less than the torque generated from samples at all frequencies. SAOS experiments were performed at 1% strain (in the linear viscoelastic regime) from 100 to 0.001 rad/s. In creep experiments, samples were subjected to constant loads at 25, 50, and 100 Pa for 30 min, and the recovery phase was monitored for 30 min after stress was removed.

In order to capture the rheological response of physical hydrogels over the entire frequency spectrum, dynamic moduli master curves were constructed using the method previously reported,[72] and the details are provided in the Supporting Information. In this study, three different models were applied to examine their efficacy in describing the rheological behaviors of gels, including the Maxwell, the stretched exponential, and the sticky Rouse models. Brief descriptions of the Maxwell and the KWW models can be found in the Supporting Information, and the sticky Rouse model has been discussed in the main text. Detailed procedures for fitting each model to the experimental data are in the Supporting Information.

■ ASSOCIATED CONTENT

Ⓢ Supporting Information

More information about the two-state model, methods for rheology data transformation, additional calculation details on estimated parameters and concentration regimes on gels, supplementary Figures S1−S12. This material is available free of charge via the Internet at http://pubs.acs.org.

■ AUTHOR INFORMATION

Corresponding Author

*bdolsen@mit.edu

Notes

The authors declare no competing financial interest.

■ ACKNOWLEDGMENTS

This research was supported by the U.S. Army Research Office through the Institute of Soldier Nanotechnologies under contract W911NF-07-D-0004. The authors would like to thank M. J. Glassman for sharing the protein genes.

■ REFERENCES

(1) Aida, T.; Meijer, E. W.; Stupp, S. I. *Science* **2012**, *335*, 813.
(2) Liu, K.; Kang, Y.; Wang, Z.; Zhang, X. *Adv. Mater.* **2013**, *25*, 5530.
(3) Guo, M.; Pitet, L. M.; Wyss, H. M.; Vos, M.; Dankers, P. Y. W.; Meijer, E. W. *J. Am. Chem. Soc.* **2014**, *136*, 6969.
(4) Albertazzi, L.; van der Zwaag, D.; Leenders, C. M. A.; Fitzner, R.; van der Hofstad, R. W.; Meijer, E. W. *Science* **2014**, *344*, 491.
(5) Cordier, P.; Tournilhac, F.; Soulie-Ziakovic, C.; Leibler, L. *Nature* **2008**, *451*, 977.
(6) Holten-Andersen, N.; Harrington, M. J.; Birkedal, H.; Lee, B. P.; Messersmith, P. B.; Lee, K. Y. C.; Waite, J. H. *Proc. Natl. Acad. Sci. U. S. A.* **2011**, *108*, 2651.
(7) Yount, W. C.; Loveless, D. M.; Craig, S. L. *J. Am. Chem. Soc.* **2005**, *127*, 14488.
(8) Rowley, J. A.; Madlambayan, G.; Mooney, D. J. *Biomaterials* **1999**, *20*, 45.
(9) Hunt, J. N.; Feldman, K. E.; Lynd, N. A.; Deek, J.; Campos, L. M.; Spruell, J. M.; Hernandez, B. M.; Kramer, E. J.; Hawker, C. J. *Adv. Mater.* **2011**, *23*, 2327.
(10) Lemmers, M.; Sprakel, J.; Voets, I. K.; van der Gucht, J.; Cohen Stuart, M. A. *Angew. Chem., Int. Ed.* **2010**, *49*, 708.
(11) Alexandridis, P.; Holzwarth, J. F.; Hatton, T. A. *Macromolecules* **1994**, *27*, 2414.
(12) Jeong, B.; Bae, Y. H.; Lee, D. S.; Kim, S. W. *Nature* **1997**, *388*, 860.
(13) Harada, A.; Kobayashi, R.; Takashima, Y.; Hashidzume, A.; Yamaguchi, H. *Nat. Chem.* **2011**, *3*, 34.
(14) Appel, E. A.; Biedermann, F.; Rauwald, U.; Jones, S. T.; Zayed, J. M.; Scherman, O. A. *J. Am. Chem. Soc.* **2010**, *132*, 14251.
(15) Schneider, J. P.; Pochan, D. J.; Ozbas, B.; Rajagopal, K.; Pakstis, L.; Kretsinger, J. *J. Am. Chem. Soc.* **2002**, *124*, 15030.
(16) Ortony, J. H.; Newcomb, C. J.; Matson, J. B.; Palmer, L. C.; Doan, P. E.; Hoffman, B. M.; Stupp, S. I. *Nat. Mater.* **2014**, *13*, 812.
(17) Nowak, A. P.; Breedveld, V.; Pakstis, L.; Ozbas, B.; Pine, D. J.; Pochan, D.; Deming, T. J. *Nature* **2002**, *417*, 424.
(18) Petka, W. A.; Harden, J. L.; McGrath, K. P.; Wirtz, D.; Tirrell, D. A. *Science* **1998**, *281*, 389.
(19) Israelachvili, J. N. *Intermolecular and surface forces*; 3rd ed.; Academic Press: Burlington, MA, 2011.
(20) Ribbeck, K.; Görlich, D. *EMBO J.* **2001**, *20*, 1320−1330.
(21) Wang, C.; Wu, H.; Chen, Z.; McDowell, M. T.; Cui, Y.; Bao, Z. *Nat. Chem.* **2013**, *5*, 1042.
(22) Tee, B. C. K.; Wang, C.; Allen, R.; Bao, Z. *Nat. Nano* **2012**, *7*, 825.
(23) Chen, Y.; Kushner, A. M.; Williams, G. A.; Guan, Z. *Nat. Chem.* **2012**, *4*, 467.
(24) Burnworth, M.; Tang, L.; Kumpfer, J. R.; Duncan, A. J.; Beyer, F. L.; Fiore, G. L.; Rowan, S. J.; Weder, C. *Nature* **2011**, *472*, 334.
(25) Sun, T. L.; Kurokawa, T.; Kuroda, S.; Ihsan, A. B.; Akasaki, T.; Sato, K.; Haque, M. A.; Nakajima, T.; Gong, J. P. *Nat. Mater.* **2013**, *12*, 932.
(26) Sun, J.-Y.; Zhao, X.; Illeperuma, W. R. K.; Chaudhuri, O.; Oh, K. H.; Mooney, D. J.; Vlassak, J. J.; Suo, Z. *Nature* **2012**, *489*, 133.
(27) Wong Po Foo, C. T. S.; Lee, J. S.; Mulyasasmita, W.; Parisi-Amon, A.; Heilshorn, S. C. *Proc. Natl. Acad. Sci. U. S. A.* **2009**, *106*, 22067.
(28) Olsen, B. D.; Kornfield, J. A.; Tirrell, D. A. *Macromolecules* **2010**, *43*, 9094.
(29) Shen, W.; Kornfield, J. A.; Tirrell, D. A. *Macromolecules* **2007**, *40*, 689.
(30) Tang, S.; Glassman, M. J.; Li, S.; Socrate, S.; Olsen, B. D. *Macromolecules* **2014**, *47*, 791.
(31) McKinnon, D. D.; Domaille, D. W.; Cha, J. N.; Anseth, K. S. *Adv. Mater.* **2014**, *26*, 865.
(32) Tanaka, F.; Edwards, S. F. *Macromolecules* **1992**, *25*, 1516.
(33) Green, M. S.; Tobolsky, A. V. *J. Chem. Phys.* **1946**, *14*, 80.
(34) Rubinstein, M.; Semenov, A. N. *Macromolecules* **1998**, *31*, 1386.
(35) Rubinstein, M.; Semenov, A. N. *Macromolecules* **2001**, *34*, 1058.
(36) Leibler, L.; Rubinstein, M.; Colby, R. H. *Macromolecules* **1991**, *24*, 4701.
(37) Cates, M. E. *Macromolecules* **1987**, *20*, 2289.
(38) Tripathi, A.; Tam, K. C.; McKinley, G. H. *Macromolecules* **2006**, *39*, 1981.
(39) Sing, M. K.; Wang, Z.-G.; McKinley, G. H.; Olsen, B. D. *Soft Matter* **2015**, *11*, 2085−2096.
(40) Gilbert, J. B.; Rubner, M. F.; Cohen, R. E. *Proc. Natl. Acad. Sci. U. S. A.* **2013**, *110*, 6651.
(41) Ader, C.; Frey, S.; Maas, W.; Schmidt, H. B.; Görlich, D.; Baldus, M. *Proc. Natl. Acad. Sci. U. S. A.* **2010**, *107*, 6281.
(42) van Meer, G.; Voelker, D. R.; Feigenson, G. W. *Nat. Rev. Mol. Cell Biol.* **2008**, *9*, 112.
(43) Stukalin, E. B.; Cai, L.-H.; Kumar, N. A.; Leibler, L.; Rubinstein, M. *Macromolecules* **2013**, *46*, 7525.
(44) Hackelbusch, S.; Rossow, T.; van Assenbergh, P.; Seiffert, S. *Macromolecules* **2013**, *46*, 6273.
(45) Rossow, T.; Habicht, A.; Seiffert, S. *Macromolecules* **2014**, *47*, 6473.

DOI: 10.1021/jacs.5b00722
J. Am. Chem. Soc. 2015, 137, 3946−3957

(46) Mi, L.; Fischer, S.; Chung, B.; Sundelacruz, S.; Harden, J. L. *Biomacromolecules* **2005**, *7*, 38.
(47) Yao, M.-H.; Yang, J.; Du, M.-S.; Song, J.-T.; Yu, Y.; Chen, W.; Zhao, Y.-D.; Liu, B. *J. Mater. Chem. B* **2014**, *2*, 3123.
(48) Collier, J. H.; Rudra, J. S.; Gasiorowski, J. Z.; Jung, J. P. *Chem. Soc. Rev.* **2010**, *39*, 3413.
(49) Wheeldon, I. R.; Gallaway, J. W.; Barton, S. C.; Banta, S. *Proc. Natl. Acad. Sci. U. S. A.* **2008**, *105*, 15275.
(50) Kim, Y. H.; Campbell, E.; Yu, J.; Minteer, S. D.; Banta, S. *Angew. Chem., Int. Ed.* **2013**, *52*, 1437.
(51) Zhang, L.; Furst, E. M.; Kiick, K. L. *J. Controlled Release* **2006**, *114*, 130.
(52) Ott, A.; Bouchaud, J. P.; Langevin, D.; Urbach, W. *Phys. Rev. Lett.* **1990**, *65*, 2201.
(53) Upadhyaya, A.; Rieu, J.-P.; Glazier, J. A.; Sawada, Y. *Phys. A (Amsterdam, Neth.)* **2001**, *293*, 549.
(54) Sprague, B. L.; Pego, R. L.; Stavreva, D. A.; McNally, J. G. *Biophys. J.* **2004**, *86*, 3473.
(55) Gunasekar, S. K.; Asnani, M.; Limbad, C.; Haghpanah, J. S.; Hom, W.; Barra, H.; Nanda, S.; Lu, M.; Montclare, J. K. *Biochemistry* **2009**, *48*, 8559.
(56) Zettl, U.; Hoffmann, S. T.; Koberling, F.; Krausch, G.; Enderlein, J.; Harnau, L.; Ballauff, M. *Macromolecules* **2009**, *42*, 9537.
(57) King, J. T.; Yu, C.; Wilson, W. L.; Granick, S. *ACS Nano* **2014**, *8*, 8802.
(58) Rubinstein, M.; Colby, R. H. *Polymer physics*; Oxford University Press: Oxford, 2003.
(59) Masaro, L.; Zhu, X. X. *Prog. Polym. Sci.* **1999**, *24*, 731.
(60) Chen, Q.; Tudryn, G. J.; Colby, R. H. *J. Rheol. (Melville, NY, U. S.)* **2013**, *57*, 1441.
(61) Chen, Q.; Liang, S.; Shiau, H.-s.; Colby, R. H. *ACS Macro Lett.* **2013**, *2*, 970.
(62) Lewis, C. L.; Stewart, K.; Anthamatten, M. *Macromolecules* **2014**, *47*, 729.
(63) Gainaru, C.; Figuli, R.; Hecksher, T.; Jakobsen, B.; Dyre, J. C.; Wilhelm, M.; Böhmer, R. *Phys. Rev. Lett.* **2014**, *112*, 098301.
(64) Indei, T.; Takimoto, J.-i. *J. Chem. Phys.* **2010**, *133*, 194902.
(65) Seitz, M. E.; Burghardt, W. R.; Faber, K. T.; Shull, K. R. *Macromolecules* **2007**, *40*, 1218.
(66) He, Y.; Lodge, T. P. *Macromolecules* **2007**, *41*, 167.
(67) Fullenkamp, D. E.; He, L.; Barrett, D. G.; Burghardt, W. R.; Messersmith, P. B. *Macromolecules* **2013**, *46*, 1167.
(68) Xu, D.; Craig, S. L. *Macromolecules* **2011**, *44*, 5465.
(69) Appel, E. A.; Forster, R. A.; Koutsioubas, A.; Toprakcioglu, C.; Scherman, O. A. *Angew. Chem., Int. Ed.* **2014**, *53*, 10038.
(70) Glassman, M. J.; Chan, J.; Olsen, B. D. *Adv. Funct. Mater.* **2013**, *23*, 1182.
(71) Glassman, M. J.; Olsen, B. D. *Soft Matter* **2013**, *9*, 6814.
(72) Tang, S.; Olsen, B. *Front. Chem.* **2014**, *2*, 23.
(73) Wang, M.; Timachova, K.; Olsen, B. D. *Macromolecules* **2013**, *46*, 1651.
(74) Schärtl, W. In *Soft Matter Characterization*; Borsali, R., Pecora, R., Eds.; Springer: Netherlands, 2008; p 677.
(75) Hamersky, M. W.; Hillmyer, M. A.; Tirrell, M.; Bates, F. S.; Lodge, T. P.; von Meerwall, E. D. *Macromolecules* **1998**, *31*, 5363.
(76) Wang, M.; Timachova, K.; Olsen, B. D. *Macromolecules* **2013**, *46*, 5694.

DOI: 10.1021/jacs.5b00722
J. Am. Chem. Soc. 2015, 137, 3946−3957